

Approximation of bone mineral density and subcutaneous adiposity using T1-weighted images of the human head

Polona Kalc¹, Felix Hoffstaedter^{4,5}, Eileen Luders^{6,7,8}, Christian Gaser^{1,2,3+}, Robert Dahnke^{1,2+}

Abstract

Bones and brain are intricately connected and scientific interest in their interaction is growing. This has become particularly evident in the framework of clinical applications for various medical conditions, such as obesity and osteoporosis. The adverse effects of obesity on brain health have long been recognised, but few brain imaging studies provide sophisticated body composition measures. Here we propose to extract the following bone- and adiposity-related measures from T1-weighted MR images of the head: an approximation of skull bone mineral density (BMD), skull bone thickness, and two approximations of subcutaneous fat (i.e., the intensity and thickness of soft non-brain head tissue). The measures pertaining to skull BMD, skull bone thickness, and intensity-based adiposity proxy proved to be reliable ($r=.93/.83/.74, p<.001$) and valid, with high correlations to DXA-derived head BMD values ($\rho=.70, p<.001$) and MRI-derived abdominal subcutaneous adipose volume ($\rho=.62, p<.001$). Thickness-based adiposity proxy had only a low retest reliability ($r=.58, p<.001$). The outcomes of this study constitute an important step towards extracting relevant non-brain features from available brain scans.

Introduction

1 The brain is closely connected to other tissues and organs (Zhou et al. 2023), including the skeletal system. A large body of literature suggests a bidirectional communication between bones and the brain (Obri et al. 2018; Rousseaud et al. 2016). Moreover, bone-derived metabolites 5 have been implicated in mood, cognition, and glucose/energy homeostasis in murine models (Guntur & Rosen 2012; Khrimian et al. 2017; Lee et al. 2007; Nakamura et al. 2021). However, the neuroimaging community largely dismisses the information from the closest bone structure surrounding the brain.

10 Bone tissue undergoes constant remodelling which is supported by osteoclasts (i.e., bone resorbing cells) and osteoblasts (i.e., new bone-forming cells) to regulate mineral homeostasis and ensure skeletal integrity (Clarke 2008; Feng and McDonald 2011). Bone metabolism is affected by endocrine signalling and innervation via the sympathetic 15 nervous system, with greater sympathetic activity leading to decreasing BMD (Ducy and Kostenuki 2015; Takeda et al. 2002). Furthermore, bone tissue actively signals to the brain and other organs and is implicated in brain metabolism by secretion of bone-derived peptides (e.g., osteocalcin, osteopontin, sclerostin, lipocalin-2, etc.), as well as by production of 20 bone marrow-derived immune cells (Chen et al. 2021; Yu et al. 2020).

The relation between BMD and fat mass is complex (Lee et al. 2020; Rinonapoli et al. 2021). For example, people with anorexia nervosa tend to have lower BMD than healthy and obese individuals (Fazeli & Klibanski 2014; Maimoun et al. 2020). However, increased adiposity levels or 25 other metabolic disorders can have a detrimental effect on bone health, as the mesenchymal stromal cells of the bone marrow in obese people preferentially convert into adipocytes (i.e. fat cells) rather than

osteoblasts (i.e. new bone-forming cells), potentially resulting in reduced bone mass (Ambrosi et al. 2017; Veldhuis-Vlug & Rosen 2018). Bone health also seems to play a role in neurodegenerative as well as neurodevelopmental disorders (Kelly et al. 2020), such as Parkinson's disease (Sleeman, Che, and Counsell 2016; Tassorelli et al. 2017), multiple sclerosis (Bisson et al. 2019), and autism spectrum disorder (Neumeyer et al. 2015). Moreover, a low BMD has been associated with an increased risk of Alzheimer's Disease (Kostev et al. 2018; Lui et al. 2003; Tan et al. 2005; Zhang et al. 2022; Zhou et al. 2011; Xiao et al. 2023).

Given the consistent reports on the connection of bone measures (e.g., BMD, bone mineral content) and brain ageing in the UK Biobank database (e.g., Miller et al. 2016; Smith et al. 2019; 2020) as well as the long-known adverse effects of obesity on cognitive and brain health (Beydoun et al. 2008; Farruggia & Small 2019), the availability of such measures in open-source brain imaging databases, such as IXI, ADNI, AIBL, or OASIS is inadequate. Here we present the extraction and validation of skull BMD, skull bone thickness, and non-brain soft head tissue thickness and intensity estimation from the head tissue classes, normally discarded when processing T1-weighted brain MR images.

Methods

Data

This research has been conducted using data from the UK Biobank (UKB application #41655), a biomedical database and research resource that contains genetic, lifestyle and health information from half a million UKB participants (<https://www.ukbiobank.ac.uk>).

¹ Structural Brain Mapping Group, Department of Neurology, Jena University Hospital, Friedrich Schiller University Jena, Germany

² Department of Psychiatry and Psychotherapy, Jena University Hospital, Friedrich Schiller University Jena, Germany

³ German Center for Mental Health (DZPG)

⁴ Forschungszentrum Jülich, Institute of Neuroscience and Medicine, Brain and Behaviour (INM-7), Germany

⁵ Institute of Systems Neuroscience, Medical Faculty, Heinrich Heine University Düsseldorf, Germany

⁶ School of Psychology, University of Auckland, Auckland, New Zealand

⁷ Department of Women's and Children's Health, Uppsala University, Uppsala, Sweden

⁸ Laboratory of Neuro Imaging, Keck School of Medicine, University of Southern California, Los Angeles, CA, USA

Corresponding authors:

Polona Kalc (polona.kalc@med.uni-jena.de),
Robert Dahnke (robert.dahnke@uni-jena.de)

+ shared last authorship

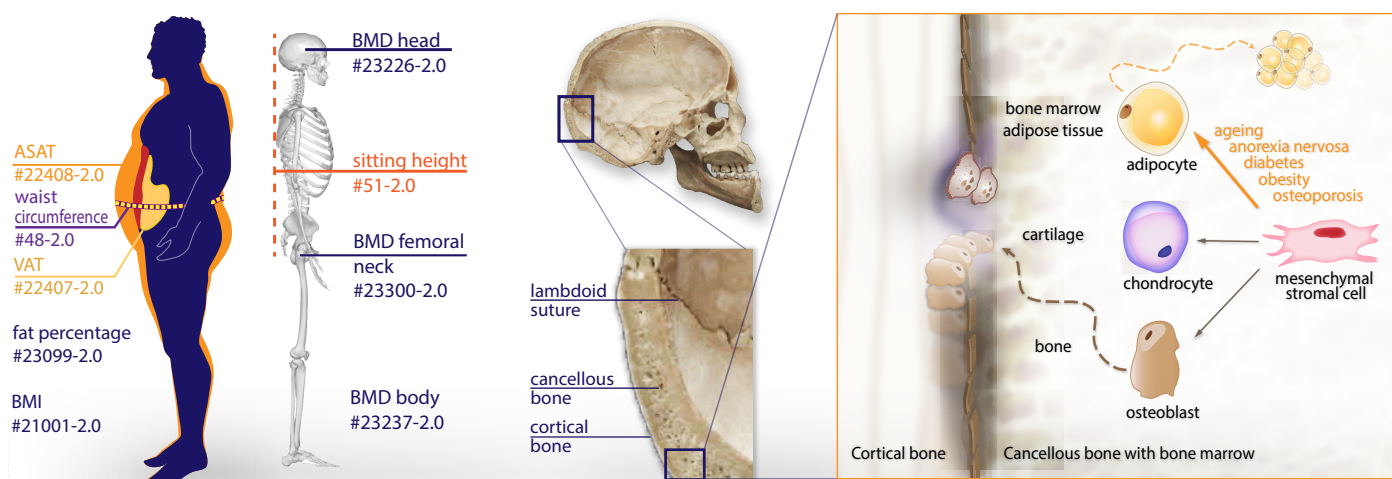


Figure 1. Demonstrates the UKB anthropometric measures used in the validation process as well as the cranial anatomy and microenvironment of a bone. Bone marrow is located within the spongy/cancellous bone (diploë). Mesenchymal stromal cells in the bone marrow have the potential to develop into osteoblasts (bone-forming cells), chondrocytes (cartilage-forming cells), or adipocytes (bone marrow fat cells). Obesity, ageing, diabetes, anorexia nervosa, starvation, and osteoporosis lead their differentiation into adipocytes and, hence, a lower BMD (Tencerova & Kassem 2016).

1 biobank.ac.uk/). The UKB has ethical approval from the North West
Multi-Centre Research Ethics Committee (MREC) and is in possession
of informed consents from the study cohort participants.
5 T1-weighted brain MR images of a subsample of healthy UKB
5 subjects ($N = 2000$, $M_{Age} = 64.17 \pm 6.34$ years, age range: 46–89 years,
50% women) were used to extract and validate our skull BMD estimate
against BMD measure of the head and total body BMD obtained by
dual energy X-ray absorptiometry (DXA) scanning. Our head tissue in-
10 tensity and thickness measures (i.e., subcutaneous fat approximation)
was evaluated with respect to body mass index, percent body fat, ab-
dominal subcutaneous adipose tissue volume (ASAT), visceral adipose
tissue volume (VAT), and waist circumference.

Furthermore, we used a sample of 316 T1-weighted MR scans
from OASIS-3 dataset, acquired at two time points within a time inter-
15 val of less than 3 months ($M_{Age} = 67.66 \pm 8.22$ years, age range: 42–85,
56% women) to determine the retest reliability of the measures for the
same as well as a (slightly) different scanners and protocols. To evaluate
the original and our refined bone segmentation, a subsample of individ-
uals with both MR and CT scans was used ($N_{CT} = 114$, $M_{Age} = 66.71 \pm$

20 8.38 years, age range: 42–85, 51% women).

The quality of the scans was monitored internally through the UKB
workflow (Alfaro-Almagro et al., 2018), and was assessed by the au-
thors in OASIS-3.

Data acquisition

Bone mineral density data acquisition

BMD measures of the head and total body were obtained by dual
25 energy X-ray absorptiometry (DXA) scanning with iDXA instrument
(GE-Lunar, Madison, WI). A detailed overview of the acquisition pro-
cedure is available in https://biobank.ndph.ox.ac.uk/showcase/ukb/docs/DXA_explan_doc.pdf.

Quantification of the subcutaneous adipose tissue

Subcutaneous adipose tissue in the abdomen was acquired by ab-
dominal MRI imaging on Siemens MAGNETOM Aera 1.5 T MRI scanner
30 (Siemens Healthineers, Erlangen, Germany) with a 6-minute dual-echo
Dixon Vibe protocol, resulting in a water and fat separated volumetric
data set (Linge et al. 2018) that was processed by AMRA Profiler Re-
search (AMRA Medical AB, Linköping, Sweden) to obtain body compo-
sition measures (Borga et al. 2015).

Brain MRI data acquisition

35 All the information regarding brain MR data acquisition is available

in the UK Biobank Imaging documentation (https://biobank.ctsu.ox.ac.uk/crystal/crystal/docs/brain_mri.pdf). In short, T1-weighted MR im-
ages were acquired on Siemens Skyra 3.0 T scanners with a 32-chan-
nel RF receive head coil. The MPRAGE sequence was used with 1-mm
isotropic resolution, inversion/repetition time = 880/2000 ms, acquisi-
tion time: 5 minutes, FOV: 208x256x256 matrix, in-plane acceleration
factor = 2.

The MRI data from the OASIS-3 dataset used in this study were
acquired on different 1.5 T and 3.0 T scanners with 20-channel head
5 coil (Siemens Sonata, Siemens TIM Trio and BioGraph mMR PET-
MR 3T) (LaMontagne et al., 2019). The MPRAGE sequence was used
with (i) 1 mm isotropic repetition/echo time = 1900/3.93 ms, FA = 15°
FOV phase = 87.50%, (ii) 1 mm isotropic inversion/repetition/echo
time = 1000/2400/3.16 ms, FA = 8°, FOV phase = 100%, R = 2 and
10 (iii) 1.20x1.05x1.05 mm resolution, inversion/repetition/echo time =
900/2300/2.95 ms, FA = 9°, FOV phase = 93.75 mm, R = 2.

CT scan data acquisition

CT scans were obtained on the Siemens Biograph 40 PET/CT scanner.
A three-second X-ray topogram was acquired in the lateral plane
and a spiral CT scan was performed for attenuation correction at the
low dose CT (LaMontagne et al. 2019).

Data preprocessing

Raw T1-weighted MR brain images were processed using SPM12
(Wellcome Center for Human Neuroimaging, <https://www.fil.ion.ucl.ac.uk/spm/>) running under Matlab 2021a (Mathworks Inc., Natick, MA,
USA), which produced the following segments: grey matter, white matter,
cerebrospinal fluid, skull, soft head tissue, and background. Of note,
instead of the default setting (3 mm), we set SPM's 'samp' parameter to
5 mm to ensure that non-brain tissues were properly classified.

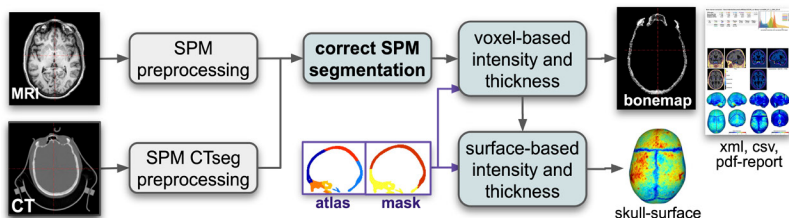
The CT data was preprocessed with CTseg utilising the unified seg-
mentation of SPM12 (Brudfors et al., 2020; <https://github.com/WCHN/CTseg>) and co-registered to the individual MRI space.

Development of the measures

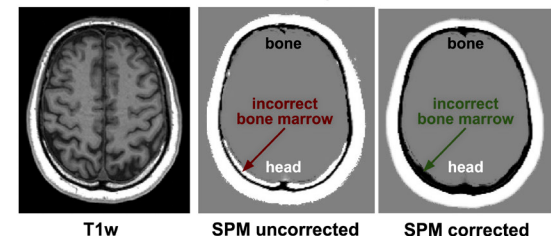
Bone measures

The SPM processing often erroneously assigned the high intensity
bone marrow to the head tissue class instead of the skull segment. Mis-
classified skull segments were therefore corrected by morphological op-
erations to avoid missing the intensities from the diploë (i.e., cancellous
(spongy) bone between the inner and outer layer of the cortical bone of

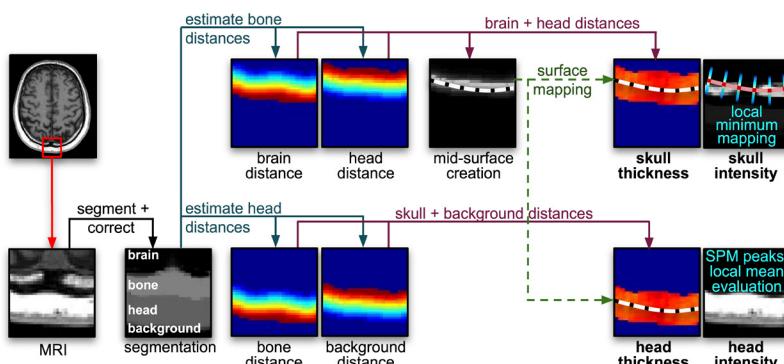
A Algorithm Data Flow Diagram



B Correction of SPM segmentation



C Bone & head measures



D Bone atlas and bone mask maps

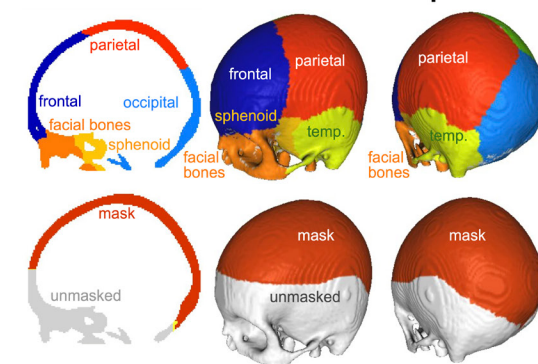


Figure 2. (A) The figure shows the workflow of the algorithm with necessary corrections (B), extraction of measures (C), and template maps (D). MRI/CT images undergo preprocessing by SPM/SPM-CTseg into CSF, GM, WM, skull, head, and background. Morphological operations are used to correct segmentation errors (B), before estimating various distance maps to describe the skull and head tissue thickness maps (C). The calvarial atlas and mask, shown in (D), are mapped to the individual space to extract regional and global values. If surface processing is required, the distance maps are used to create a percentage position map, which allows the creation of the mid-skull-surface. This surface is then used to map the local thickness, intensity and atlas region to the surface to extract a regional or masked global thickness and intensity value.

1 the skull) and to correct the underestimated bone thickness (Figure 2B).

- *Intensity-based measures*

Bone measures were derived from the corrected SPM skull segment, by quantifying the mean intensity across the entire segment labelled as skull (or within a specific skull region), and normalised by the 5 SPM-derived WM intensity.

- *Thickness-based measures*

Bone thickness was defined as the sum of the shortest distance from each skull voxel to the CSF and to the soft non-brain head tissue.

In addition to voxel-based processing, a midline surface was generated to map bone values along the surface-normal. This allowed the 10 cortical bone intensity, quantified as the local minimum, to be separated from the bone marrow intensity, defined as the distance-weighted average of the mapped points (Figure 2C).

Head tissue measures

- *Intensity-based measures*

To approximate the adipose tissue of the head, we estimated as a weighted average of the SPM-derived Gaussian peaks by their proportions in the tissue class labelled as head. Head tissue intensity was described as a percentage composite of the various soft non-brain head tissues.

- *Thickness-based measures*

Local head thickness was calculated as the shortest distance from each soft head tissue voxel to the skull and to the background. 20 The sum of both distances then yielded the estimate of the voxel-wise head tissue thickness. A separation into different head tissues (i.e., muscle, skin, and fat) was omitted because of varying amounts of (chemical shift) artefacts and inhomogeneities across the image. Of note, the lower portions of all brain scans as well as 25 voxels located more than 30 mm from the skull were excluded from the head tissue thickness estimation to avoid side effects due to

defacing and/or varying scanning protocols and procedures.

1

Boney Atlas

The processing results yielded clearly identifiable coronal, sagittal and lambdoid sutures, visibly separating the calvarial bones. We therefore created a template atlas of the skull regions by averaging affine and intensity-normalised T1-weighted images as well as CT data of OASIS-3, and manually labelling the skull segment tissue probability map using Slicer3D (Fedorov et al. 2012; <https://slicer.readthedocs.io/en/5.0/index.html>). The atlas was mapped into individual space using the linear transformation from the SPM segmentation. Additionally, we created a bone mask to avoid critical regions that are often affected by defacing or are in parts very thin, such as temporal and sphenoid bones (Figure 2D). The identified bone regions were used in extracting regional bone and adiposity measures.

5

10

15

20

25

30

Validation of the measures

The segmentation results were visually examined against ground truth CT data, juxtaposing MR- and CT-derived measures from the OASIS-3 dataset (see Figure S1 in the Supplement^{**}).

Global and regional measures were tested to obtain the best estimates of the BMD in an exploratory manner on a subsample of 1000 subjects ($M_{Age} = 64.02 \pm 6.40$ years, age range: 46–80 years, 50% women). A random forest regression with all the extracted bone measures as independent variables predicting the UKB head's BMD measure and a permutation test were run in R (version 4.3.3; R Core Team 2022) with packages *party* (Hothorn et al., 2006) and *flexplot* (Fife, 2022). The final BMD approximation measure was chosen based on the estimated predictor importance values from a permutation test (Fife & D'Onofrio, 2023).

The selected measures were validated by calculating the Spearman correlation coefficient (*psych* package; Revelle, 2024) to relevant measures available in the UKB in a subsample of 1000 subjects not included in the exploratory analysis ($M_{Age} = 63.81 \pm 6.27$ years, age range: 46–79 years, 50% women). We calculated the associations with head BMD (UKB #23226-2.0) and total body BMD (UKB #23237-2.0), as well

1 as body fat percentage (UKB #23099-2.0) and abdominal subcutaneous adipose tissue (UKB #22408-2.0) volume, for the estimates of skull
2 BMD and head tissue thickness, respectively (see Figure 1[”]).
3 We additionally inspected the correlation to other anthropo-
4 metric and lifestyle variables that had previously been connected
5 to BMD or adiposity (Cusano, 2015; Molenaar et al. 2009; Shojaa
6 et al. 2020; Ward & Klesges, 2001; Williams et al., 2005). We in-
7 vestigated the association with BMI (UKB #21001-2.0), sitting
8 height (UKB #51-2.0), visceral adipose tissue volume (VAT; UKB
9 #22407-2.0), waist circumference (UKB #48-2.0), and BMD of the
10 left femoral neck (UKB #23300-2.0). Furthermore, we included the
11 variables connected to physical activity, namely duration of mod-
12 erate (UKB #894-2.0) and vigorous physical activity (UKB #914-
13 2.0), as well as pack years of smoking as proportion of life span
14 exposed to smoking (UKB #20162-2.0) and frequency of alcohol
15 intake (UKB #1558-2.0).

As an additional validation step, we performed a volume-based morphometry (VBM) analysis in SPM12 with BMD of the head and our newly extracted proxy BMD as predictors of the extracted
20 warped and smoothed (FWHM = 8 mm) intensity-normalised skull segments on the whole sample of 2000 UKB subjects.

Evaluation of reliability

We calculated the retest reliability of the estimated measures using T1-weighted images from the OASIS-3 dataset acquired at two time points within an interval of less than 3 months. One
25 subject was excluded from the analysis due to a failed SPM-seg-
mentation, resulting in a total sample of 157 subjects (age range:
42–85, $M_{Age} = 67.64 \pm 8.24$ years, 55% women). The reliability of
the measures was estimated under the same scanner/protocol
and mixed scanner/protocol conditions.

Results

Validation of the measures on the UK Biobank dataset

The results of the exploratory step showed that the most relevant measure for the BMD approximation is the mean intensity extracted from the occipital bone (Table S1 in the Supplement[”]). The results were confirmed by the VBM analysis of the skull segments, where we could see the highest association of the head BMD and the occipital region
35 of the skull (Figure 4[”]). We assumed the same pattern for the head tis-
sue thickness and intensity estimates based on visual inspection of the images. All further analyses therefore included the occipital measures to represent the skull BMD, skull bone thickness, intensity-based, and thickness-based adiposity proxies.

The validation results against other anthropometric and lifestyle measures are shown in Figure 3C (and Figure S2 in the Supplement[”]). The extracted measures showed valid associations to other UKB pa-
rameters. The Spearman's correlation coefficients between the extract-
ed proxy BMD measure and UKB-derived head BMD were .70, .72, and
45 .67 for a total sample, women, and men, respectively (see Figure S3[”] in
the Supplement for the bootstrapped correlation coefficient). The cor-
relation with the total body BMD was moderate for the total sample and the subsample of men ($\rho = .64$ and $.57$, respectively, $p < .0001$) and higher for women ($\rho = .72$, $p < .0001$). The association to other anthro-
50 metric measures showed a weak negative correlation with total fat percent ($\rho = -.14$, $p < .01$), and a low positive correlation with waist circumference ($\rho = .15$, $p < .01$). A weak negative association between the proxy BMD measure and the exposure to smoking was observed in a subsample of men ($\rho = -.12$, $p < .01$). Bone thickness (in the occipi-
55 tal part) was, on the other hand, weakly associated with body composition measures in men (ASAT: $\rho = .31$, $p < .0001$; waist circumference:

$\rho = .31$, $p < .0001$, percent body fat: $.30$, $p < .0001$).

Our intensity-based adiposity approximation was moderately to highly positively correlated with other body composition measures. The Spearman's correlation coefficients with BMI were .52, .52, and .57 for a total sample, women, and men, respectively. The association is higher for a volume of visceral adipose tissue (VAT), namely .57, .68, and .70 for a total sample, women, and men, respectively, and abdominal subcutaneous adipose tissue volume (ASAT; $\rho = .62$; $\rho = .64$; $\rho = .65$, for a total sample, women, and men, respectively). Similar patterns were observed in our thickness-based adiposity approximation. The measure was moderately positively associated with other body composition measures. The Spearman's correlation coefficients with BMI were .50, .54, and .48 for a total sample, women, and men, respectively. The association with VAT volume was higher, namely .65, .56, and .45 for a total sample, women, and men, respectively. The thickness-based adiposity proxy had a similar correlation with VAT as BMI in a total sample ($\rho = .65$, $p < .0001$; $\rho = .64$, $p < .0001$ for VAT association with head thickness and BMI, respectively), but lower in subsamples of men and women (see Figure S2 in the Supplement[”]).

It could be observed that the measures were biased due to anthropometric differences between the biological sexes. For subsequent use in statistical analyses, the sex, age and TIV of the participants must be taken into account.

The reliability of the measures (OASIS-3)

The retest reliability based on the data obtained with the same pro-
tocol on two different time-points ($n = 63$, $M_{Age} = 69.27 \pm 7.32$ years,
48–85, 54% women) was high for the skull BMD ($r = .93$; $p < .001$) and bone thickness estimation ($r = .83$, $p < .001$), comparatively to the re-
gional GM volume ($r = .98$, $p < 0.001$). Our thickness-based adiposity proxy showed lower retest reliability ($r = .58$, $p < .001$). Nevertheless,
the intensity-based adiposity proxy had a sufficient reliability of .74 ($p < .001$). It should be noted that the retest reliability of the measures de-
rived from images acquired with different protocols is generally lower
than for identical protocols. The results from the whole selected sam-
ple ($n = 157$) and varying protocols between the two time-points ($n = 94$, $M_{Age} = 66.91 \pm 8.81$ years, 42–85, 50% women) are available in the
Supplementary Table S2[”].

Discussion

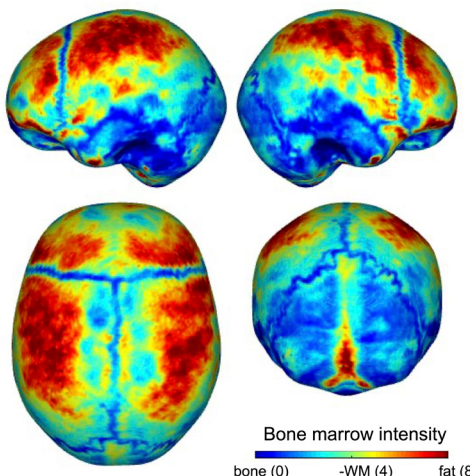
In the present study, we used tissue classes that are typically dis-
carded when processing brain images to estimate skull BMD, skull bone
thickness, as well as intensity- and thickness-based adiposity approx-
imations. Such measures are normally not considered in neuroimaging
research. However, burgeoning research shows the interconnect-
edness between brain, bones, and adipose tissue (Caron et al., 2018;
Rousseaud et al., 2016). Thus, the aim of this new line of research is
to provide the neuroimaging community with proxy measures that can
be extracted from standard T1-weighted brain scans that are available
in open-source databases or that have been acquired by researchers
following standard protocols of brain imaging.

Reliability and validity of measures

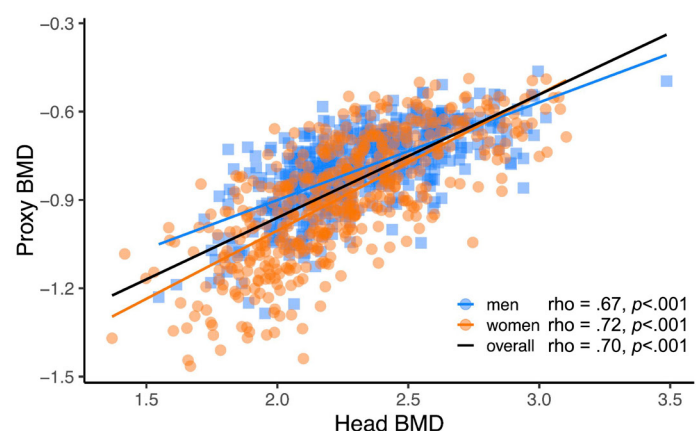
All extracted measures showed a good retest reliability on the
OASIS-3 dataset in both same- and mixed-protocol test cases, with the
only exception of thickness-based adiposity proxy. Its low retest reliabil-
ity might be due to bias introduced during the head segment correction,
and further development is currently underway to improve this specific
measurement.

The validity of the proxy BMD measure was confirmed by moderate
to high associations with DXA-derived BMD measures of the head
and total body. The proxy BMD measure also showed a link to age in
women (but not men). This is expected as women experience signifi-
cant changes in bone mass with ageing due to decreases in oestrogen

A Extracted skull surface



B Association of head BMD and estimated skull BMD for women and men



C Correlation plot of the extracted skull and fat measures, the original UKB measures and SPM-derived relative brain tissue volumes

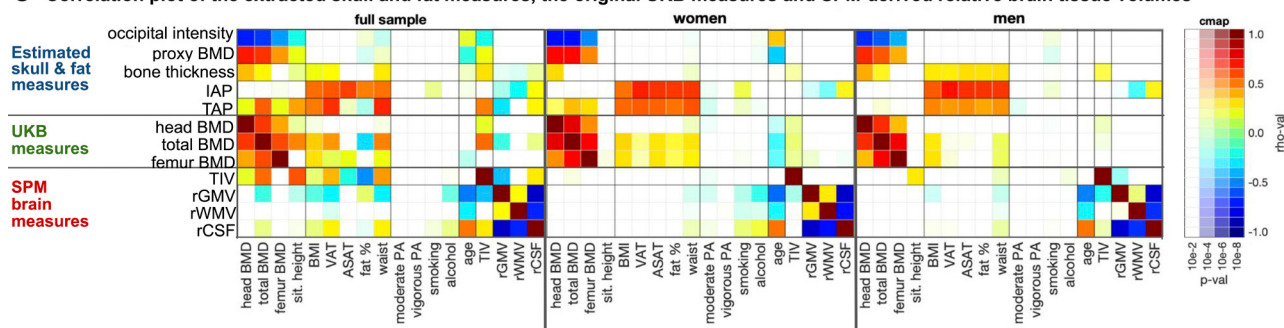


Figure 3. (A) The extracted skull surface of a subject from the UK Biobank with visible sutures and high intensity bone marrow. (B) Scatterplot of the UKB head BMD and our skull BMD estimate for men and women. Higher head BMD is related to lower (occipital) bone intensity in the MRI and therefore results in a higher proxy BMD value. (C) Spearman correlation coefficients with Holm correction for multiple comparisons between the estimated skull BMD proxy, bone thickness, as well as intensity- and thickness-based adiposity proxies (IAP & TAP, respectively), and other UKB and brain measures. The extracted measures are associated with the original BMD as well as body composition measures.

and increases of follicle-stimulating hormone (Almeida, 2012; Iqbal et al. 2012). Men, on the other hand, are less susceptible to age-related hormonal fluctuations, and their bone mass tends to remain stable until later in life (Porter & Varacallo, 2022). However, certain medications and poor lifestyle choices (e.g., physical inactivity or smoking) can also increase the risk of developing osteoporosis in men (Porter & Varacallo, 2022). In fact, our proxy BMD measure was partly linked to smoking exposure in men.

The validity of skull bone thickness was confirmed by association with certain aspects of body composition measures. Higher BMI and abdominal adiposity were weakly related to higher skull bone thickness in the occipital region. These results could be linked to the body weight-related mechanical stress to the bone (Cherukuri et al. 2021). However, it is typically the lean body mass that has a positive effect on bone health, rather than fat mass (Ho-Pham et al., 2014; Nguyen et al., 2020). Nevertheless, the connection between skull bone thickness and adiposity might involve the effects of adipokines (i.e., cytokines produced by the adipocytes) on bone mass (Mangion et al. 2023) and further studies are needed to elucidate this finding.

The associations of thickness- and intensity-based adiposity proxy measures with UKB anthropometric measures are moderate to high; BMI had the lowest correlation and waist circumference and VAT the highest. This lower connection to BMI is not surprising, as BMI is inherently a proxy measure of body composition (Gutin, 2018). Among other drawbacks, BMI fails to account for changes in body composition when ageing, where lean muscle mass typically decreases while visceral adiposity increases, resulting in no change in weight (Bhurosy & Jeewon 2013). In an ageing sample like the UKB, such limited association to BMI is expected. Nevertheless, a stronger association between thickness-based adiposity proxy with VAT (in comparison to BMI) is crucial, as it shows the relevance of its extraction for the approximation of

abdominal obesity. Moreover, both adiposity proxy measures were also negatively correlated with the relative GM volume and positively with CSF volume, which corroborates the previous findings on the negative influence of obesity on brain structure (Gómez-Apo et al., 2021).

Potential application

Previous studies have shown that head fat tissue volume is linked to estimates of body composition in people with obesity (Wang et al. 2014). Nevertheless, to our knowledge, we conducted the first study that provides an estimate of BMD from a T1-weighted scan of the head. The outcomes of our study suggest that skull BDM can serve as a proxy measure of a person's total BMD. In addition, the information on skull bone thickness might become relevant in studies of traumatic brain injuries as the cranium plays a vital role in protecting the brain (Semple & Panagiotopoulou, 2023). Furthermore, the thickness-based adiposity proxy measures can be included as potential confounds in functional neuroimaging studies, such as electroencephalography, functional near infrared spectroscopy, and transcranial direct current stimulation (Gorniak et al. 2022). Last but not least, the adiposity proxy measures may provide valuable information beyond the typically used BMI, which has several limitations (Burkhauser & Cawley 2008; Tomiyama et al. 2016), especially when used in cohorts of older individuals (Bhurosy & Jeewon 2013; Rothman 2008). This might be particularly relevant as many open-source brain imaging databases (e.g., ADNI, AIBL, OASIS) include a high percentage of adults who are past midlife.

Limitations and future directions

The bone and adiposity estimations derived from T1-weighted MRI scans are not suitable for clinical use. This is especially relevant as structural MRI protocols can vary in fat-suppression intensity, which can affect the estimates in various ways. Characterising the nature

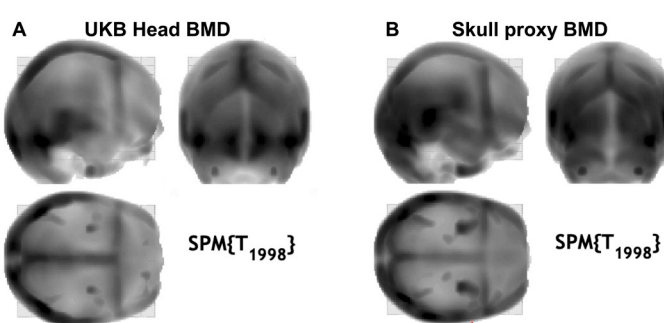


Figure 4. 'Glass' head maps from the VBM analysis in SPM with (A) head BMD from the UKB as a predictor of the intensity-normalised skull segments, and (B) proxy BMD measure as a predictor of the intensity-normalised skull segments.

1 of these variations and developing robust estimations for MRI protocols with fat suppression is warranted in future studies. Additionally, our proxy BMD measure is highly correlated with head BMD, but only moderately with the BMD of femoral neck, which is a better predictor of
5 fracture risk (Kanis et al. 2004). With its high morbidity and mortality in older adults and its association to AD, fracture risk is a relevant aspect of healthy ageing (Friedman et al., 2010). Thus, future studies utilising machine learning might focus on establishing a better predictor of (femoral neck) BMD. Moreover, deep learning might aid in segmenting specific tissue classes, such as muscles, skin, and fat, which could result in an even better (skinfold-like) approximation of an individual's status related to overall health as well as obesity (Langner et al. 2020; Leong et al. 2024). Altogether, the present study serves as a pilot exploring the potential value of non-brain tissue analyses in the field of neuroimaging.
10 Further studies are necessary to improve and validate the measures.
15

Data and code availability statement

The data used for this work were obtained from the UK Biobank Resource (Project Number 41655). Due to the nature of the data sharing agreement, we are not allowed to publish the data. The OASIS-3 dataset is openly available at <https://www.oasisbrains.org>. Prior to accessing the data, users are required to agree to the OASIS data use terms (DUT), which follow the creative commons attribution 4.0 licence. The code developed in this study is available on GitHub: <https://github.com/robdaahn/boney>

Authorship contribution statement

Polona Kalc: Conceptualization, Formal analysis, Validation, Writing – original draft, Writing – review and editing, Visualisation. **Felix Hoffstaedter:** Resources, Data curation, Writing – review & editing. **Eileen Luders:** Writing – review & editing. **Christian Gaser:** Supervision, Funding acquisition, Writing – review & editing. **Robert Dahne:** Conceptualization, Software, Data curation, Validation, Visualisation, Writing – review & editing.

Funding

The study was supported by Carl Zeiss Stiftung as a part of the IMPULS project (IMPULS P2019-01-006), the Federal Ministry of Science and Education (BMBF) under the frame of ERA PerMed (Pattern-Cog ERAPERMED2021-127), and the Marie Skłodowska-Curie Innovative Training Network (SmartAge 859890 H2020-MSCA-ITN2019).

Declaration of Competing Interests

The authors declare no conflict of interest.

Acknowledgements

This research has been conducted using data from UK Biobank under the application number 41655. We gratefully acknowledge the time and effort of the UK Biobank participants as well as the researchers and staff involved in data collection and management.

Data were provided in part by OASIS-3: Longitudinal Multimodal Neuroimaging: Principal Investigators: T. Benzinger, D. Marcus, J. Morris; NIH P30 AG066444, P50 AG00561, P30 NS09857781, P01 AG026276, P01 AG003991, R01 AG043434, UL1 TR000448, R01 EB009352. AV-45 doses were provided by Avid Radiopharmaceuticals, a wholly owned subsidiary of Eli Lilly.

References

- Alfaro-Almagro, F., Jenkinson, M., Bangerter, N. K., Andersson, J. L. R., Griffanti, L., Douaud, G., Sotiropoulos, S. N., Jbabdi, S., Hernandez-Fernandez, M., Vallee, E., Vidaurre, D., Webster, M., McCarthy, P., Rorden, C., Daducci, A., Alexander, D. C., Zhang, H., Dragouni, I., Matthews, P. M., ... Smith, S. M. (2018). Image processing and Quality Control for the first 10,000 brain imaging datasets from UK Biobank. *NeuroImage*, 166, 400–424. <https://doi.org/10.1016/j.neuroimage.2017.10.034>
- Almeida, M. (2012). Aging mechanisms in bone. *BoneKEy Reports*, 1(7). <https://doi.org/10.1038/bonekey.2012.102>
- Ambrosi, T. H., Scialdone, A., Graja, A., Gohlke, S., Jank, A.-M., Bocian, C., Woelk, L., Fan, H., Logan, D. W., Schürmann, A., Saraiva, L. R., & Schulz, T. J. (2017). Adipocyte Accumulation in the Bone Marrow during Obesity and Aging Impairs Stem Cell-Based Hematopoietic and Bone Regeneration. *Cell Stem Cell*, 20(6), 771-784.e6. <https://doi.org/10.1016/j.stem.2017.02.009>
- Beydoun, M. A., Beydoun, H. A., & Wang, Y. (2008). Obesity and central obesity as risk factors for incident dementia and its subtypes: A systematic review and meta-analysis. *Obesity Reviews*, 9(3), 204–218. <https://doi.org/10.1111/j.1467-789X.2008.00473.x>
- Bhurosy, T., & Jeewon, R. (2013). Pitfalls of Using Body Mass Index (BMI) in Assessment of Obesity Risk. *Current Research in Nutrition and Food Science Journal*, 1(1), 71–76. <https://doi.org/10.12944/CRNFSJ.1.1.07>
- Bisson, E. J., Finlayson, M. L., Ekuma, O., Leslie, W. D., & Marrie, R. A. (2019). Multiple sclerosis is associated with low bone mineral density and osteoporosis. *Neurology: Clinical Practice*, 9(5), 391–399. <https://doi.org/10.1212/CPJ.0000000000000669>
- Borga, M., Thomas, E. L., Romu, T., Rosander, J., Fitzpatrick, J., Dahlqvist Leinhard, O., & Bell, J. D. (2015). Validation of a fast method for quantification of intra-abdominal and subcutaneous adipose tissue for large-scale human studies: Quantification of IAAT and ASAT. *NMR in Biomedicine*, 28(12), 1747–1753. <https://doi.org/10.1002/nbm.3432>
- Brudfors, M., Balbastre, Y., Flandin, G., Nachev, P., & Ashburner, J. (2020). Flexible Bayesian Modelling for Nonlinear Image Registration. In A. L. Martel, P. Abolmaesumi, D. Stoyanov, D. Mateus, M. A. Zuluaga, S. K. Zhou, D. Racocceanu, & L. Joskowicz (Eds.), *Medical Image Computing and Computer Assisted Intervention – MICCAI 2020* (Vol. 12263, pp. 253–263). Springer International Publishing. <https://doi.org/10.1007/978-3-030-59716-0-25>
- Burkhauser, R. V., & Cawley, J. (2008). Beyond BMI: The value of more accurate measures of fatness and obesity in social science research. *Journal of Health Economics*, 27(2), 519–529. <https://doi.org/10.1016/j.jhealeco.2007.05.005>
- Caron, A., Lee, S., Elmquist, J. K., & Gautron, L. (2018). Leptin and brain-adipose crosstalks. *Nature Reviews Neuroscience*, 19(3), 153–165. <https://doi.org/10.1038/nrn.2018.7>
- Chen, H., Shang, D., Wen, Y., & Liang, C. (2021). Bone-Derived Modulators That Regulate Brain Function: Emerging Therapeutic Targets for Neurological Disorders. *Frontiers in Cell and Developmental Biology*, 9, 683457. <https://doi.org/10.3389/fcell.2021.683457>
- Cherukuri, L., Kinninger, A., Birudaraju, D., Lakshmanan, S., Li, D., Flores, F., Mao, S., & Budoff, M. J. (2021). Effect of body mass index on bone mineral density is age-specific. *Nutrition, Metabolism and Cardiovascular Diseases*, 31(6),

- 1767–1773. <https://doi.org/10.1016/j.numecd.2021.02.027>
- Clarke, B. (2008). Normal Bone Anatomy and Physiology. *Clinical Journal of the American Society of Nephrology*, 3(Supplement 3), S131–S139. <https://doi.org/10.2215/CJN.04151206>
- Cusano, N. E. (2015). Skeletal Effects of Smoking. *Current Osteoporosis Reports*, 13(5), 302–309. <https://doi.org/10.1007/s11914-015-0278-8>
- Ducy, P., & Kostenuik, S. (2015). Leptin and Bone. In S. Dagogo-Jack, MD (Ed.), *Leptin* (pp. 145–161). Springer International Publishing. https://doi.org/10.1007/978-3-319-09915-6_12
- Farruggia, M. C., & Small, D. M. (2019). Effects of adiposity and metabolic dysfunction on cognition: A review. *Physiology & Behavior*, 208, 112578. <https://doi.org/10.1016/j.physbeh.2019.112578>
- Fazeli, P. K., & Klibanski, A. (2014). Bone Metabolism in Anorexia Nervosa. *Current Osteoporosis Reports*, 12(1), 82–89. <https://doi.org/10.1007/s11914-013-0186-8>
- Fedorov, A., Beichel, R., Kalpathy-Cramer, J., Finet, J., Fillion-Robin, J.-C., Pujol, S., Bauer, C., Jennings, D., Fennessy, F., Sonka, M., Buatti, J., Aylward, S., Miller, J. V., Pieper, S., & Kikinis, R. (2012). 3D Slicer as an image computing platform for the Quantitative Imaging Network. *Magnetic Resonance Imaging*, 30(9), 1323–1341. <https://doi.org/10.1016/j.mri.2012.05.001>
- Feng, X., & McDonald, J. M. (2011). Disorders of Bone Remodeling. *Annual Review of Pathology: Mechanisms of Disease*, 6(1), 121–145. <https://doi.org/10.1146/annurev-pathol-011110-130203>
- Fife, D. (2022). Flexplot: Graphically-based data analysis. *Psychological Methods*, 27(4), 477–496. <https://doi.org/10.1037/met0000424>
- Fife, D.A. & D'Onofrio, J. (2023). Common, uncommon, and novel applications of random forest in psychological research. *Behav Res* 55, 2447–2466. <https://doi.org/10.3758/s13428-022-01901-9>
- Friedman, S. M., Menzies, I. B., Bukata, S. V., Mendelson, D. A., & Kates, S. L. (2010). Dementia and Hip Fractures: Development of a Pathogenic Framework for Understanding and Studying Risk. *Geriatric Orthopaedic Surgery & Rehabilitation*, 1(2), 52–62. <https://doi.org/10.1177/2151458510389463>
- Gómez-Apo, E., Mondragón-Maya, A., Ferrari-Díaz, M., & Silva-Pereyra, J. (2021). Structural Brain Changes Associated with Overweight and Obesity. *Journal of Obesity*, 2021, 1–18. <https://doi.org/10.1155/2021/6613385>
- Gorniak, S. L., Meng, H., & Pollonini, L. (2022). Correlation between subcutaneous adipose tissue of the head and body mass index: Implications for functional neuroimaging. *Human Movement Science*, 85, 102997. <https://doi.org/10.1016/j.humov.2022.102997>
- Guntur, A. R., & Rosen, C. J. (2012). Bone As An Endocrine Organ. *Endocrine Practice*, 18(5), 758–762. <https://doi.org/10.4158/EP12141.RA>
- Gutin, I. (2018). In BMI we trust: Reframing the body mass index as a measure of health. *Social Theory & Health*, 16(3), 256–271. <https://doi.org/10.1057/s41285-017-0055-0>
- Hothorn, T., Hornik, K., Zeileis, A. (2006). Unbiased Recursive Partitioning: A Conditional Inference Framework. *Journal of Computational and Graphical Statistics*, 15(3), 651–674. doi:10.1198/106186006X133933
- Ho-Pham, L. T., Nguyen, U. D. T., & Nguyen, T. V. (2014). Association Between Lean Mass, Fat Mass, and Bone Mineral Density: A Meta-analysis. *The Journal of Clinical Endocrinology & Metabolism*, 99(1), 30–38. <https://doi.org/10.1210/jc.2013-3190>
- Iqbal, J., Blair, H. C., Zallone, A., Sun, L., & Zaidi, M. (2012). Further evidence that FSH causes bone loss independently of low estrogen. *Endocrine*, 41(2), 171–175. <https://doi.org/10.1007/s12020-012-9626-y>
- Kanis, J. A., Borgstrom, F., De Laet, C., Johansson, H., Johnell, O., Jonsson, B., Oden, A., Zethraeus, N., Pfleger, B., & Khaltaev, N. (2005). Assessment of fracture risk. *Osteoporosis International*, 16(6), 581–589. <https://doi.org/10.1007/s00198-004-1780-5>
- Kelly, R. R., Sidles, S. J., & LaRue, A. C. (2020). Effects of Neurological Disorders on Bone Health. *Frontiers in Psychology*, 11, 612366. <https://doi.org/10.3389/fpsyg.2020.612366>
- Khrimian, L., Obri, A., Ramos-Brossier, M., Rousseaud, A., Moriceau, S., Nicot, A.-S., Mera, P., Kosmidis, S., Karnavas, T., Saudou, F., Gao, X.-B., Oury, F., Kandel, E., & Karsenty, G. (2017). Gpr158 mediates osteocalcin's regulation of cognition. *Journal of Experimental Medicine*, 214(10), 2859–2873. <https://doi.org/10.1084/jem.20171320>
- Kostev, K., Hadji, P., & Jacob, L. (2018). Impact of Osteoporosis on the Risk of Dementia in Almost 60,000 Patients Followed in General Practices in Germany. *Journal of Alzheimer's Disease*, 65(2), 401–407. <https://doi.org/10.3233/JAD-180569>
- Langner, T., Strand, R., Ahlström, H., & Kullberg, J. (2020). Large-scale biometry with interpretable neural network regression on UK Biobank body MRI. *Scientific Reports*, 10(1), 17752. <https://doi.org/10.1038/s41598-020-74633-5>
- LaMontagne, P. J., Benzinger, T. L., Morris, J. C., Keefe, S., Hornbeck, R., Xiong, C., Grant, E., Hassenstab, J., Moulder, K., Vlassenko, A. G., Raichle, M. E., Cruchaga, C., & Marcus, D. (2019). OASIS-3: Longitudinal Neuroimaging, Clinical, and Cognitive Dataset for Normal Aging and Alzheimer Disease [Preprint]. *Radiology and Imaging*. <https://doi.org/10.1101/2019.12.13.19014902>
- Lee, N. J., Qi, Y., Enriquez, R. F., Clarke, I., Ip, C. K., Wee, N., Baldock, P. A., & Herzog, H. (2020). Energy partitioning between fat and bone mass is controlled via a hypothalamic leptin/NPY relay. *International Journal of Obesity*, 44(10), 2149–2164. <https://doi.org/10.1038/s41366-020-0550-6>
- Lee, N. K., Sowa, H., Hinoi, E., Ferron, M., Ahn, J. D., Confavreux, C., Dacquin, R., Mee, P. J., McKee, M. D., Jung, D. Y., Zhang, Z., Kim, J. K., Mauvais-Jarvis, F., Ducy, P., & Karsenty, G. (2007). Endocrine Regulation of Energy Metabolism by the Skeleton. *Cell*, 130(3), 456–469. <https://doi.org/10.1016/j.cell.2007.05.047>
- Leong, L. T., Wong, M. C., Liu, Y. E., Glaser, Y., Quon, B. K., Kelly, N. N., Cataldi, D., Sadowski, P., Heymsfield, S. B., & Shepherd, J. A. (2024). Generative deep learning furthers the understanding of local distributions of fat and muscle on body shape and health using 3D surface scans. *Communications Medicine*, 4(1), 13. <https://doi.org/10.1038/s43856-024-00434-w>
- Linge, J., Borga, M., West, J., Tuthill, T., Miller, M. R., Dumitriu, A., Thomas, E. L., Romu, T., Tunón, P., Bell, J. D., & Dahlqvist Leinhard, O. (2018). Body Composition Profiling in the UK Biobank Imaging Study. *Obesity*, 26(11), 1785–1795. <https://doi.org/10.1002/oby.22210>
- Lui, L.-Y., Stone, K., Cauley, J. A., Hillier, T., & Yaffe, K. (2003). Bone Loss Predicts Subsequent Cognitive Decline in Older Women: The Study of Osteoporotic Fractures. *Journal of the American Geriatrics Society*, 51(1), 38–43. <https://doi.org/10.1034/j.1601-5215.2002.51007.x>
- Maimoun, L., Garnero, P., Mura, T., Nocca, D., Lefebvre, P., Philibert, P., Seneque, M., Gaspari, L., Vauchot, F., Courtet, P., Sultan, A., Piketty, M.-L., Sultan, C., Renard, E., Guillaume, S., & Mariano-Goulart, D. (2020). Specific Effects of Anorexia Nervosa and Obesity on Bone Mineral Density and Bone Turnover in Young Women. *The Journal of Clinical Endocrinology & Metabolism*, 105(4), e1536–e1548. <https://doi.org/10.1210/clinem/dgz259>
- Mangion, D., Pace, N. P., & Formosa, M. M. (2023). The relationship between adipokine levels and bone mass—A systematic review. *Endocrinology, Diabetes & Metabolism*, 6(3), e408. <https://doi.org/10.1002/edm2.408>
- Miller, K. L., Alfaro-Almagro, F., Bangerter, N. K., Thomas, D. L., Yacoub, E., Xu, J., Bartsch, A. J., Jbabdi, S., Sotiroopoulos, S. N., Andersson, J. L. R., Griffanti, L., Douaud, G., Okell, T. W., Weale, P., Dragoni, I., Garratt, S., Hudson, S., Collins, R., Jenkinson, M., ... Smith, S. M. (2016). Multimodal population brain imaging in the UK Biobank prospective epidemiological study. *Nature Neuroscience*, 19(11), 1523–1536. <https://doi.org/10.1038/nn.4393>
- Molenaar, E. A., Massaro, J. M., Jacques, P. F., Pou, K. M., Ellison, R. C., Hoffmann, U., Pencina, K., Shadwick, S. D., Vasan, R. S., O'Donnell, C. J., & Fox, C. S. (2009). Association of Lifestyle Factors With Abdominal Subcutaneous and Visceral Adiposity. *Diabetes Care*, 32(3), 505–510. <https://doi.org/10.2337/dc08-1382>
- Nakamura, M., Imaoka, M., & Takeda, M. (2021). Interaction of bone and brain: Osteocalcin and cognition. *International Journal of Neuroscience*, 131(11), 1115–1123. <https://doi.org/10.1080/00207454.2020.1770247>
- Neumeyer, A. M., O'Rourke, J. A., Massa, A., Lee, H., Lawson, E. A., McDougle, C. J., & Misra, M. (2015). Brief Report: Bone Fractures in Children and Adults with Autism Spectrum Disorders. *Journal of Autism and Developmental Disorders*, 45(3), 881–887. <https://doi.org/10.1007/s10803-014-2228-1>
- Nguyen, H. G., Pham, M. T., Ho-Pham, L. T., & Nguyen, T. V. (2020). Lean mass and peak bone mineral density. *Osteoporosis and Sarcopenia*, 6(4), 212–216.

- <https://doi.org/10.1016/j.afos.2020.10.001>
- Obri, A., Khrimian, L., Karsenty, G., & Oury, F. (2018). Osteocalcin in the brain: From embryonic development to age-related decline in cognition. *Nature Reviews Endocrinology*, 14(3), 174–182. <https://doi.org/10.1038/nrendo.2017.181>
- Porter, J.L. & Varacallo, M. (2022). Osteoporosis [Updated August 4, 2023]. StatPearls. StatPearls Publishing. Retrieved March 18, 2024 from <https://www.ncbi.nlm.nih.gov/books/NBK441901/>
- R Core Team (2022). R: A language and environment for statistical computing. R Foundation for Statistical Computing, Vienna, Austria. <https://www.R-project.org/>
- Revelle, W. (2024). psych: Procedures for Psychological, Psychometric, and Personality Research. Northwestern University, Evanston, Illinois. R package version 2.4.3, <https://CRAN.R-project.org/package=psych>.
- Rinonapoli, G., Pace, V., Ruggiero, C., Ceccarini, P., Bisaccia, M., Meccariello, L., & Caraffa, A. (2021). Obesity and Bone: A Complex Relationship. *International Journal of Molecular Sciences*, 22(24), 13662. <https://doi.org/10.3390/ijms222413662>
- Rothman, K. J. (2008). BMI-related errors in the measurement of obesity. *International Journal of Obesity*, 32(S3), S56–S59. <https://doi.org/10.1038/ijo.2008.87>
- Rousseaud, A., Moriceau, S., Ramos-Brossier, M., & Oury, F. (2016). Bone-brain crosstalk and potential associated diseases. *Hormone Molecular Biology and Clinical Investigation*, 28(2). <https://doi.org/10.1515/hmbci-2016-0030>
- Semple, B. D., & Panagiotopoulou, O. (2023). Cranial Bone Changes Induced by Mild Traumatic Brain Injuries: A Neglected Player in Concussion Outcomes? *Neurotrauma Reports*, 4(1), 396–403. <https://doi.org/10.1089/neur.2023.0025>
- Shojaa, M., Von Stengel, S., Schoene, D., Kohl, M., Barone, G., Bragonzoni, L., Dallolio, L., Marini, S., Murphy, M. H., Stephenson, A., Mänty, M., Julin, M., Risto, T., & Kemmler, W. (2020). Effect of Exercise Training on Bone Mineral Density in Post-menopausal Women: A Systematic Review and Meta-Analysis of Intervention Studies. *Frontiers in Physiology*, 11, 652. <https://doi.org/10.3389/fphys.2020.00652>
- Sleeman, I., Che, Z. C., & Counsell, C. (2016). Risk of fracture amongst patients with Parkinson's disease and other forms of parkinsonism. *Parkinsonism & Related Disorders*, 29, 60–65. <https://doi.org/10.1016/j.parkreldis.2016.05.026>
- Smith, S. M., Elliott, L. T., Alfaro-Almagro, F., McCarthy, P., Nichols, T. E., Douaud, G., & Miller, K. L. (2020). Brain aging comprises many modes of structural and functional change with distinct genetic and biophysical associations. *eLife*, 9, e52677. <https://doi.org/10.7554/eLife.52677>
- Smith, S. M., Vidaurre, D., Alfaro-Almagro, F., Nichols, T. E., & Miller, K. L. (2019). Estimation of brain age delta from brain imaging. *NeuroImage*, 200, 528–539. <https://doi.org/10.1016/j.neuroimage.2019.06.017>
- Takeda, S., Elefteriou, F., Levasseur, R., Liu, X., Zhao, L., Parker, K. L., Armstrong, D., Ducy, P., & Karsenty, G. (2002). Leptin Regulates Bone Formation via the Sympathetic Nervous System. *Cell*, 111(3), 305–317. [https://doi.org/10.1016/S0092-8674\(02\)01049-8](https://doi.org/10.1016/S0092-8674(02)01049-8)
- Tan, Z. S., Seshadri, S., Beiser, A., Zhang, Y., Felson, D., Hannan, M. T., Au, R., Wolf, P. A., & Kiel, D. P. (2005). Bone Mineral Density and the Risk of Alzheimer Disease. *Archives of Neurology*, 62(1), 107. <https://doi.org/10.1001/archneur.62.1.107>
- Tassorelli, C., Berlangieri, M., Buscone, S., Bolla, M., De Icco, R., Baricich, A., Pacchetti, C., Cisari, C., & Sandrini, G. (2017). Falls, fractures and bone density in Parkinson's disease – a cross-sectional study. *International Journal of Neuroscience*, 127(4), 299–304. <https://doi.org/10.1080/00207454.2016.1206897>
- Tencerova, M. & Kassem, M. (2016). The Bone Marrow-Derived Stromal Cells: Commitment and Regulation of Adipogenesis. *Front Endocrinol*, 21(7), 127. doi: 10.3389/fendo.2016.00127
- Tomiyama, A. J., Hunger, J. M., Nguyen-Cuu, J., & Wells, C. (2016). Misclassification of cardiometabolic health when using body mass index categories in NHANES 2005–2012. *International Journal of Obesity*, 40(5), 883–886. <https://doi.org/10.1038/ijo.2016.17>
- Veldhuis-Vlug, A. G., & Rosen, C. J. (2018). Clinical implications of bone marrow adiposity. *Journal of Internal Medicine*, 283(2), 121–139. <https://doi.org/10.1111/j.1365-2796.2017.22011.x>
- joimj.12718
- Wang, X., Liu, H., Huang, Y., Sun, H., Bu, L., & Qu, S. (2014). Head fat is a novel method of measuring metabolic disorder in Chinese obese patients. *Lipids in Health and Disease*, 13(1), 113. <https://doi.org/10.1186/1476-511X-13-113>
- Ward, K. D., & Klesges, R. C. (2001). A meta-analysis of the effects of cigarette smoking on bone mineral density. *Calcified Tissue International*, 68(5), 259–270. <https://doi.org/10.1007/BF02390832>
- Williams, F. M. K. (2005). The effect of moderate alcohol consumption on bone mineral density: A study of female twins. *Annals of the Rheumatic Diseases*, 64(2), 309–310. <https://doi.org/10.1136/ard.2004.022269>
- Xiao, T., Ghatal, S., Mooldijk, S. S., Trajanoska, K., Oei, L., Gomez, M. M., Ikram, M. K., Rivadeneira, F., & Ikram, M. A. (2023). Association of Bone Mineral Density and Dementia: The Rotterdam Study. *Neurology*, 100(20), e2125–e2133. <https://doi.org/10.1212/WNL.00000000000207220>
- Yu, Z., Ling, Z., Lu, L., Zhao, J., Chen, X., Xu, P., & Zou, X. (2020). Regulatory Roles of Bone in Neurodegenerative Diseases. *Frontiers in Aging Neuroscience*, 12, 610581. <https://doi.org/10.3389/fnagi.2020.610581>
- Zhang, X., Hsu, W. W. Q., Sing, C.-W., Li, G. H. Y., Tan, K. C. B., Kung, A. W. C., Wong, J. S. H., Wong, I. C.-K., & Cheung, C.-L. (2022). Low Bone Mineral Density With Risk of Dementia: A Prospective Cohort Study. *Journal of the American Medical Directors Association*, 23(10), 1719.e9–1719.e19. <https://doi.org/10.1016/j.jamda.2022.07.012>
- Zhou, R., Deng, J., Zhang, M., Zhou, H.D., Wang, Y.J. (2011). Association between bone mineral density and the risk of Alzheimer's disease. *J Alzheimers Dis*, 24(1), 101–108. doi: 10.3233/JAD-2010-101467.
- Zhou, W., Zhao, L., Mao, Z., Wang, Z., Zhang, Z., & Li, M. (2023). Bidirectional Communication Between the Brain and Other Organs: The Role of Extracellular Vesicles. *Cellular and Molecular Neurobiology*, 43(6), 2675–2696. <https://doi.org/10.1007/s10571-023-01345-5>

Supplementary material

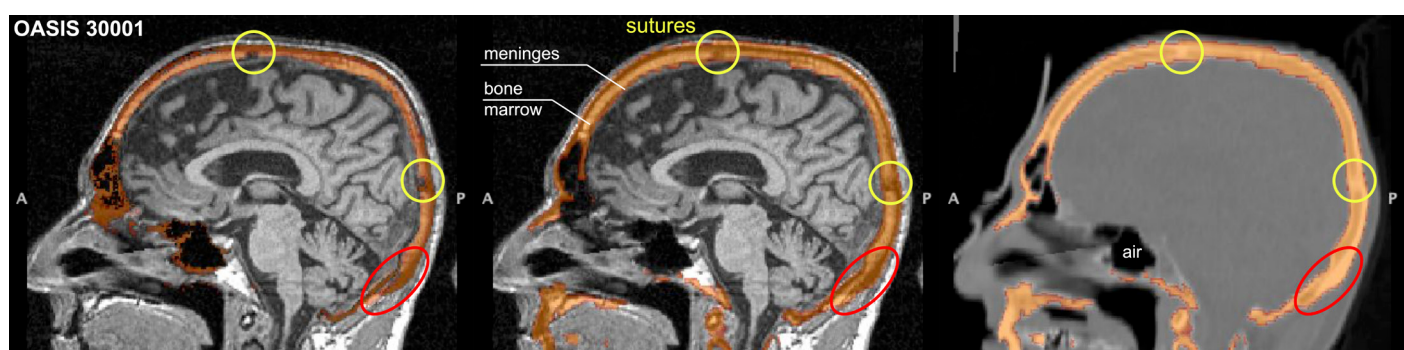


Figure S1. (A) Segmentation result of an OASIS-3 subject for MRI and CT. Overlap of the original SPM MRI segmentation (left) and the CTseg CT segmentation on the MRI (middle) and the co-registered CT images. The general overlap of the MRI and CT image is very good. The oversegmentation of the skull on the top of the head could indicate light chemical shift artefacts. Details of the bone structure are visible in both, CT and MRI, where sutures (yellow circles) are darker in MRI but brighter in CT, and the bone marrow is brighter in MRI but darker in CT (also in case of fat suppression) (red).

Table S1. Results of the best predictor estimation in 5 folds.

Fold	Best predictor 1 [variable importance]	Best predictor 2 [variable importance]	Best predictor 3 [variable importance]	Variance explained by the model
1	sROI_bonecortex01 0.053	main_sBMDH 0.051	sROI_bonethickness03 0.051	0.62
2	sROI_bonecortex03 0.052	vROI_bonethickness01 0.047	sROI_bonecortex01 0.045	0.60
3	sROI_bonecortex03 0.052	main_sBMDH 0.051	sROI_bonethickness03 0.043	0.60
4	sROI_bonecortex03 0.061	main_sBMDH 0.056	sROI_bonecortex01 0.055	0.65
5	main_sBMDH 0.054	sROI_bonecortex04 0.051	sROI_bonecortex03 0.051	0.63

Notes. sROI_bonecortex01: surface-based global bone intensity value, sROI_bonecortex03: surface-based occipital bone intensity value, sROI_bonecortex04: surface-based right parietal bone intensity value; sROI_bonethickness03: thickness of the occipital bone;

main_sBMDH is the opposite value of the sROI_bonecortex03 (mean occipital bone intensity value);

Variable importance: difference in RMSE of the model using predicted vs. permuted observations (Fife & D'Onofrio, 2023).

Table S2. Pearson's correlation coefficient for OASIS-3 rescans within 3 months ($p < 0.001$). The images were mostly acquired on different Siemens scanners with slightly different protocols independent of the time point which introduce variations comparable to independent sites.

Measures	Full sample (N = 157)	Same protocol (N = 63)	Mixed protocols (N = 94)
Occipital bone intensity (sROI_bonecortex03)	0.71	0.93	0.71
Occipital bone thickness (sROI_bonethickness03)	0.81	0.83	0.79
SPM head tissue class intensity (tis_head)	0.67	0.74	0.59
Occipital head thickness (sROI_headthickness03)	0.45	0.58	0.51
Relative GM volume (rGMV)	0.94	0.98	0.90

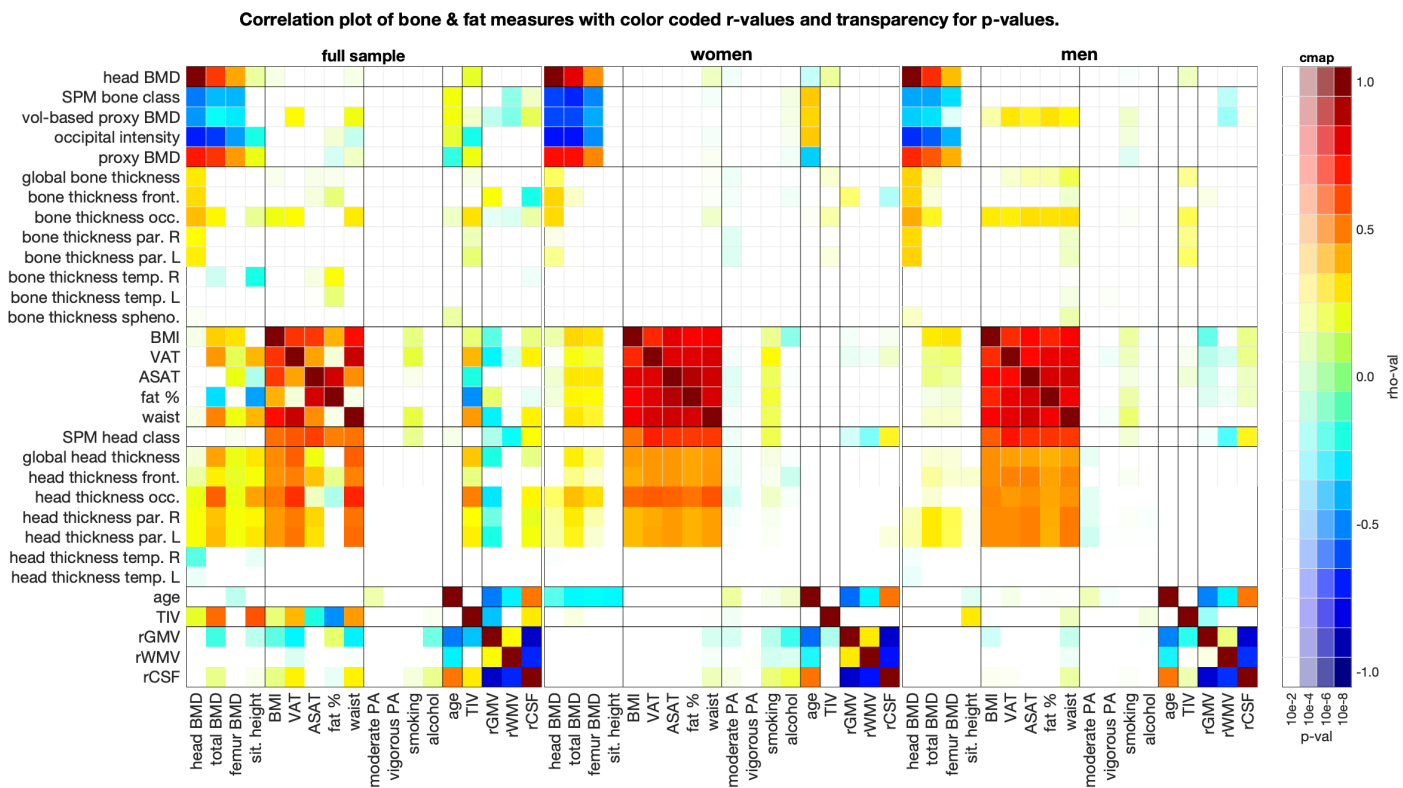


Figure S2. Spearman correlation coefficients with Holm correction for multiple comparisons between the estimated skull BMD proxy, head thickness, and other UKB and brain measures. SPM bone class represents a weighted average of the 3 Gaussian curves estimated by the SPM in the bone class. Vol-based proxy BMD is the volume-derived estimation of the bone intensity in the occipital bone. Proxy BMD is the opposite value of the surface-derived estimation of the bone intensity in the occipital bone.

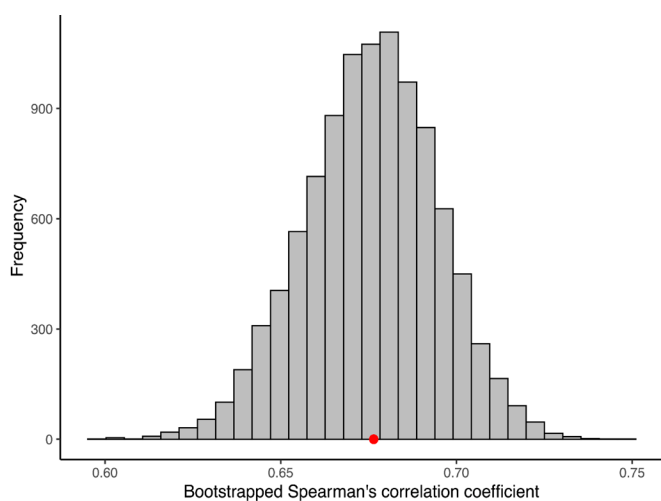


Figure S3. A distribution of bootstrapped Spearman's correlation coefficients between the proxy BMD measure and DXA-derived head BMD. The red dot represents the Bootstrap estimated correlation coefficient ($\rho = 0.68$, $p < 0.001$, 95% CI 0.64–0.71).

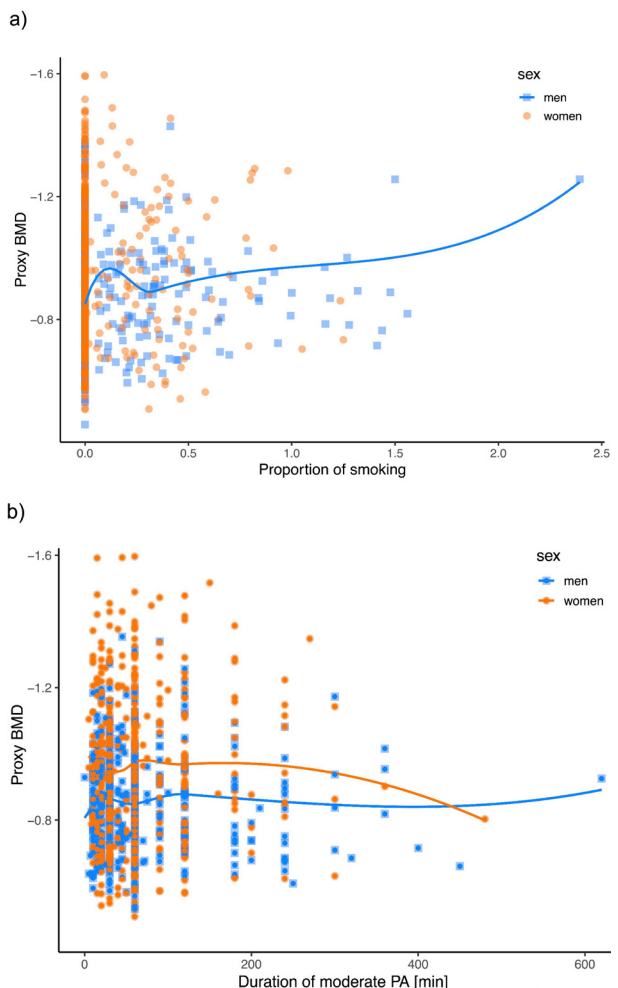


Figure S4. The association of proxy BMD measure and a) the amount of smoking and b) duration of physical activity for men and women. The negative effects of smoking are more evident in men, whereas positive effects of moderate physical activity are more prominent in women.

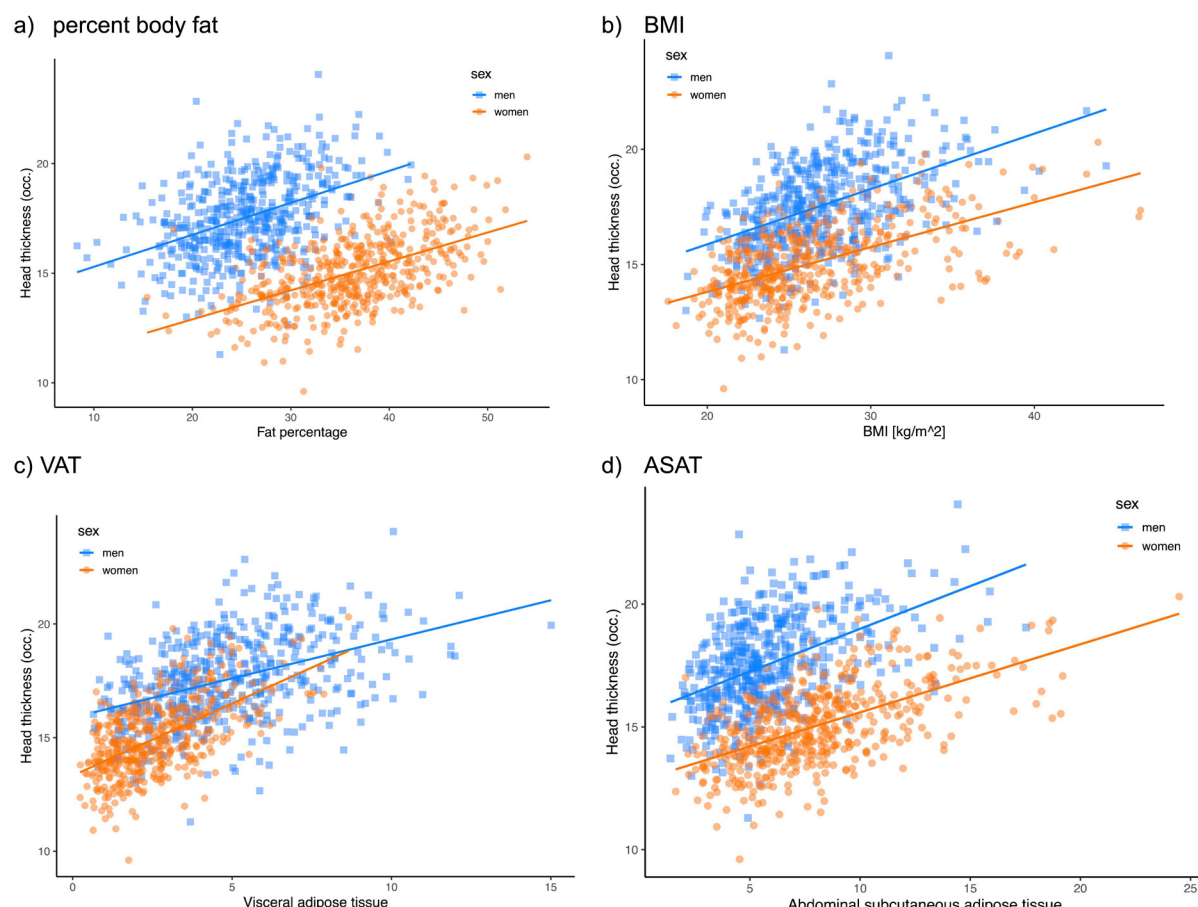


Figure S5. The association between head thickness estimation in the occipital part and **a)** percent body fat, **b)** BMI, **c)** VAT (visceral adipose tissue), and **d)** ASAT (abdominal subcutaneous adipose tissue).

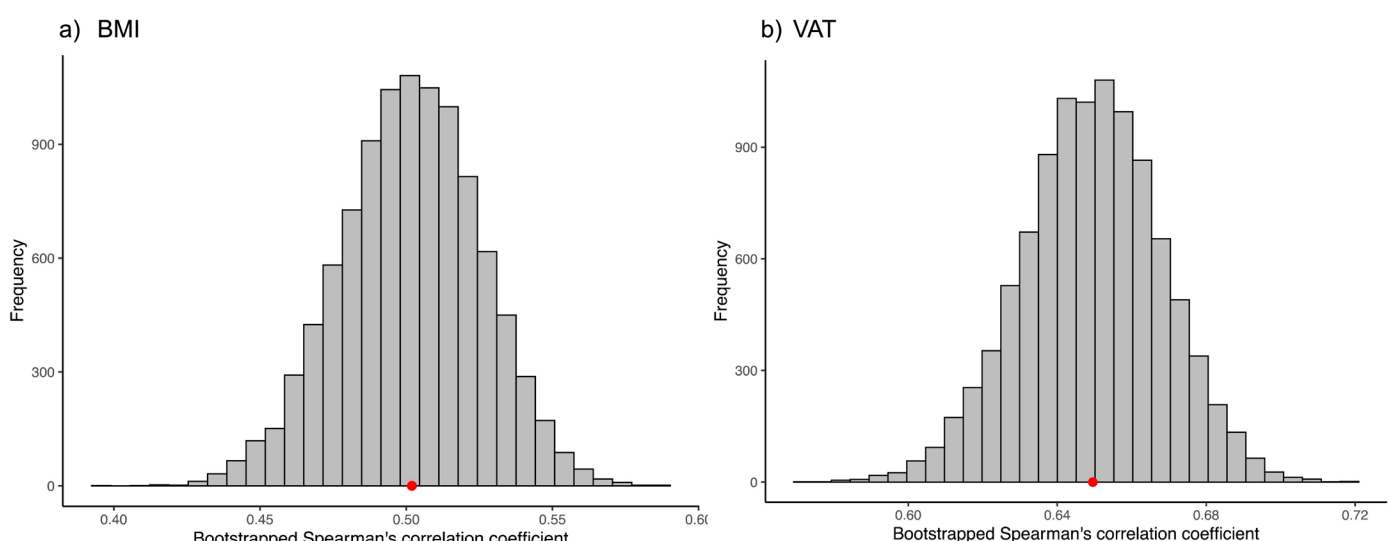


Figure S6. Bootstrapped Spearman's correlation coefficients between the head thickness approximation and the a) BMI ($\rho = 0.50$, $p < .001$, 95% CI: 0.45–0.55) and b) VAT ($\rho = 0.65$, $p < .001$, 95% CI: 0.61–0.69).